sustainability

MDPI

Article

Integration of Phase Change Material into PV Windows to Improve the Efficiency of Semi-Transparent Panels Based on Luminescent Solar Concentrator Technology

Giulio Mangherini [1,*], Eleonora Baccega [2], Valentina Diolaiti [1] and Donato Vincenzi [1,3]

[1] Department of Physics and Earth Sciences, University of Ferrara, v. G. Saragat 1, 44122 Ferrara, FE, Italy; valentina.diolaiti@unife.it (V.D.); donato.vincenzi@unife.it (D.V.)
[2] Department of Architecture, University of Ferrara, v. Quartieri 8, 44121 Ferrara, FE, Italy; eleonora.baccega@unife.it
[3] Consorzio Futuro in Ricerca, v. G. Saragat 1, 44122 Ferrara, FE, Italy
* Correspondence: giulio.mangherini@unife.it

Abstract: This research addresses the need for enhanced thermal management in building-integrated photovoltaic systems, specifically focusing on semi-transparent PV panels based on luminescent solar concentrator (LSC) technology. In pursuit of optimal thermal regulation, the cooling effect of a paraffin PCM was investigated via finite element simulations developed with COMSOL Multiphysics. The PCM was thermally coupled with the PV cells situated in the frame of a south-facing window. Due to the seasonal difference between winter and summer, the PCM latent heat capacity and melting temperature were optimized to ensure the maximum nominal operating cell temperature (NOCT) reduction during summer months. PCM latent heat capacities equivalent to 120 kJ/kg, 180 kJ/kg, and 240 kJ/kg have been investigated, whereas for the melting temperature a range from 20 °C to 42 °C was spanned. The combination of higher latent heat and 36 °C melting point showed the most significant thermal benefits, by reducing the NOCT from 42 °C to 36 °C, which led to an 11.80% increase in power output across the whole PV window. Considering the same latent heat, the other melting temperature resulted in more moderate benefits, namely an enhancement of 7.88% and 3.94%, for 38 °C and 40 °C, respectively. The lower latent heat capacities resulted in an NOCT reduction that ranged between 2.7 °C and 5.3 °C, according to the associated melting point. These results testify that the presented solution could significantly enhance energy production in semi-transparent PV applications based on LSC panels.

Keywords: solar windows; building-integrated photovoltaics (BIPVs); energy efficiency; luminescent solar concentrators (LSCs); phase change materials (PCMs); photovoltaic thermal management

Citation: Mangherini, G.; Baccega, E.; Diolaiti, V.; Vincenzi, D. Integration of Phase Change Material into PV Windows to Improve the Efficiency of Semi-Transparent Panels Based on Luminescent Solar Concentrator Technology. *Sustainability* **2024**, *16*, 11148. https://doi.org/10.3390/su162411148

Academic Editor: Yuanda Cheng

Received: 12 November 2024
Revised: 5 December 2024
Accepted: 17 December 2024
Published: 19 December 2024

1. Introduction

The achievement of the objectives recommended by the European Union within 2050 is necessarily related to a higher penetration of renewable energy sources in covering building energy demand. Indeed, the building sector is responsible for almost 40% of global CO_2 emissions and energy consumption, considering both commercial and residential buildings [1]. The evolution of this sector is focused on developing buildings that are highly energy-efficient, often termed nearly zero-energy buildings. A key factor in achieving this goal is the integration of photovoltaic (PV) technologies, whose widespread adoption demonstrates its versatility in applications such as water heating, decontamination, and electricity generation [2,3]. Solar windows are a great example of this approach. They combine photovoltaic functionality with the building envelope, directly reducing energy demand and supporting nearly zero-energy building design goals [4]. Although it is not the most efficient semi-transparent PV solution, luminescent solar concentrators (LSCs) have suitable features for building integration, especially in the urban context. The main

advantage of LSCs lies in their high transparency, which ensures, in several illumination conditions, an elevated indoor comfort with electricity production at the same time [5,6].

An LSC module consists of a pane, made of plastic or glass that, thanks to the presence of luminescent species, absorbs a portion of the sunlight impinging on the slab. The absorbed light is emitted via fluorescence by the luminophores and concentrated onto PV cells optically coupled to the panel edges, via total internal reflection. The presence of a waveguiding component between the solar radiation and the PV cells confers unique properties to LSC panels, such as their ability to convert with the same efficiency both direct and diffuse radiation, and their high tolerance to shading [7]. While acting as energy active components, LSC panels present a high architectural flexibility [8]. Therefore, the realization of PV windows based on LSC panels represents a promising solution to support further expansion of building-integrated photovoltaic (BIPV) devices, especially if coupled with high energy density storage technologies [9]. Figure 1 presents a diagram schematizing the working principles of an LSC panel. Typically, a BIPV fenestration based on LSC panels consists of two glass windows, and while the solar energy transmission can vary depending on the fluorophore concentration, the overall heat transfer coefficient remains comparable to the one of standard double-glazing solutions [10].

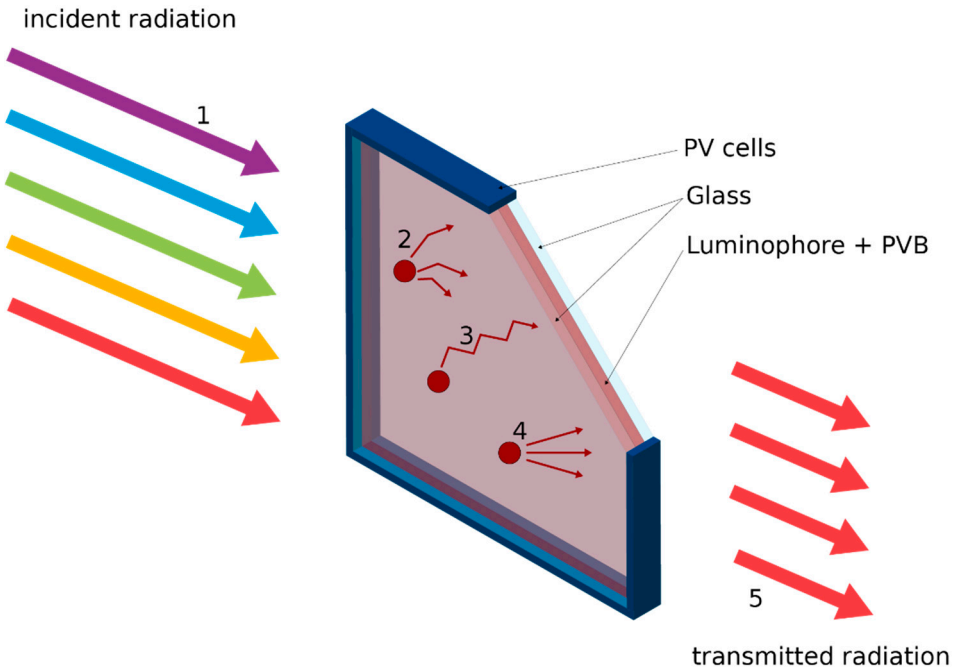

Figure 1. Schematic of LSC functioning presenting the panel used in this work. (1) Solar irradiance impinging on the semi-transparent waveguide. (2) Fluorophores absorbing the impinging radiation and re-emitting it within the waveguide. (3) Fluorescence light guided to the slab edges via total internal reflection (net of waveguide absorption). (4) Fluorescence light exiting the slab via escape cone. (5) Transmitted light.

Due to their high transparency, LSC panels are characterized by a modest electrical efficiency if compared to traditional semi-transparent PV devices [11]. In literature, there are several examples aiming to investigate the impact of different components on the LSC panel efficiency [12–14]; however, the utilization of low-cost components plays a pivotal role for the industrial scalability of these panels. For this reason, in LSC panels designed for BIPV solutions, organic dyes and Si PV cells are employed instead of more efficient, but expensive components [15]. An effective approach to improving the overall efficiency of these devices, without directly modifying their main components, is the mitigation of parasitic effects impacting device performance [16]. An interesting solution is the one proposed by Liu et al. [17], who presented a PV window based on an LSC in

which the escape cone losses were mitigated thanks to the presence of a thermotropic material in the indoor side. This additional layer significantly increased the module output power (25%) but decreased the panel transmittance by 43.3%. An alternative solution to increase the panel performance without influencing its transmittance is the thermal management of PV cells. The solutions designed to lower the operating temperature of PV modules are generally categorized into active or passive cooling methods [18]. The former offers consistent cooling potential, but with the added complexity of pumps, pipelines, as well as the requirement for regular maintenance [19]. The latter improves the thermal performance of PV modules by leveraging various physical principles without the need for regular maintenance or external energy input [20]. Phase Change Materials (PCMs) fall into the second category, and their impact on traditional PV panels has been extensively studied [21,22], with numerous experiments demonstrating their significant cooling potential [23,24]. A large body of research highlights how properly selected PCMs can effectively reduce the operating temperature of photovoltaic modules [25,26]. These materials have the potential to provide relevant temperature reductions for extended periods of time [27] and, contrary to other passive methods, they have the advantage of being independent from the installation layout [28]. The thermal coupling of PCMs with PV panels not only reduces nominal operating cell temperature (NOCT) but it delays its increasing rate. Indeed, the PCM thermally manages the PV module, acting as a heat sink, as the overheating produced by the PV cells is absorbed by the PCM upon reaching its melting temperature (PCM charging phase). In the discharging phase, the PCM releases the stored thermal energy, transitioning from liquid back to solid state [29]. As the PCM discharges, the heat it releases mitigates sharp drops in temperature, preventing excessive cooling of the PV panels [30]. Considering that when the temperature of crystalline silicon PV cells exceeds 25 °C, power generation efficiency is affected by a derating factor ranging from 0.4%/°C to −0.65%/°C [31], the inclusion of PCMs in LSC panels may considerably increase its performance.

Most studies focusing on the integration of PCMs in windows present double-glazed structures, in which the PCMs are either inserted in the air chamber between the glasses [32,33], or incorporated in the blinds and shutter components [34]. While embedding PCMs within double-glazed units offers considerable energy-saving potential, this approach is associated with high fabrication and maintenance costs, as well as the risk of material leakage. Conversely, integrating PCMs in other window components, like the shutters, provides a cost-effective alternative that avoids structural modifications, and supports flexible usage, resulting in more practical solutions for widespread applications [35]. The effect of PCMs on a semi-transparent PV window was studied by Karthick et al. [36,37]. Their measurements revealed that the inclusion of PCM led to instantaneous temperature reductions of up to 12 °C. Over the year, this cooling effect translated into an 8% relative increase in electrical yield, highlighting the significant impact of PCM integration on improving PV module performance. However, the custom-design module was based on a spaced-type structure integrating traditional crystalline silicon solar cells [38], in which the PCM was embedded between the two glasses. In these structures, the cells are typically arranged with spaces between them to allow light to pass through [39]. Their energy conversion efficiency remains close to conventional opaque PV panels, but the light transmission is sacrificed, making them less suitable for applications where higher transparency is needed [40]. Mittal et al. [41] investigated the combination of a specific PCM and LSC to enhance its electrical efficiency. The PCM thermal regulation increases LSC efficiency by up to 3%, a significant improvement over the panel standalone efficiency of 1%. Nevertheless, they performed simulations in which the LSC panel was treated as a standalone object, without considering the impact of environmental parameters or the thermal inertia of the building envelope on the NOCT.

In this work, the impact of PCMs on the efficiency of a highly transparent PV window realized with an LSC panel was evaluated. The presented semi-transparent device has solar cells coupled only on the slab edges, so as to design a PV panel having a non-patterned

and continuous optical surface similar to a standard window. The LSC panel device was integrated on the outer layer of a double-glazing PV window, and the effect of a paraffin PCM on the NOCT was estimated via thermal simulations developed with the software "COMSOL Multiphysics" 6.1. The PCM was placed inside the window frame in direct contact with the PV arrays, thus preventing the problems related to the presence of the PCM in the double-glazing. Moreover, to ensure a comprehensive correlation between the NOCT and the thermal inertia of the building envelope, the window frame was simulated as encased in a two-headed wall. Under these conditions, a parametric study on PCM physical properties was conducted by varying both its melting temperature and specific heat, assessing the PCM performance during heating and cooling seasons.

The following section presents the methodology used to perform the simulations. Section 3 presents the obtained results, displaying the relationship between the cooling potential provided by the PCM and its effect on the electrical performance of the PV window. Section 4 elaborates on the outlook for future research, and Section 5 concludes the work.

2. Material and Methods

COMSOL Multiphysics 6.1 is a software platform designed to simulate complex physical systems using a hierarchical structure. The simulations were carried out through a 3D model, where the PV window was represented with boundary conditions that change over time. The model created in COMSOL enabled the analysis of the temperature distribution of the PV arrays placed at the four LSC edges. The system thermal behavior has been simulated thanks to the "Heat transfer in Solid and Fluids" (HT) node, which models the conduction phenomena. To correctly simulate conduction phenomena, HT requires the thermal properties of the components inserted in the models, in particular the material thermal conductivity, λ, density ρ, and heat capacity at constant pressure c_p. These parameters have been defined by using COMSOL library, whereas to correlate the NOCT to both the PCM, latent heat (Δh) and melting temperature (T_{melt}) were used as simulation parameters. For the former, the values of 120 kJ/kg, 180 kJ/kg, and 240 kg/kg were investigated, while the latter was varied from 20 °C to 42 °C with steps of 2 °C. Lastly, the PCM melting range was supposed to be equivalent to 3 °C. The summary of the thermal properties attributed to each component is listed in Table 1.

Table 1. Thermal properties of the material used in the simulations.

	ρ [kg/m^3]	**λ [W/(m·K)]**	**c_p kJ/(kg·K)]**	**Δh [kJ/kg]**	**T_{melt} [°C]**
PCM	600	0.2	2000	120 ÷ 240	20 ÷ 42
Wall	1600	0.5	800	ND	ND
Window frame	1300	0.4	1800	ND	ND
Glass	2203	1.38	703	ND	ND
PVB film	1180	0.19	1466	ND	ND
Solar cells	2330	165	677	ND	ND

ND = not defined.

The LSC panel was modeled as a glazed waveguide presenting a total thickness of 7 mm, in which the red dye was integrated thanks to a thin layer having the thermal properties of an ~1 mm polyvinyl butyral (PVB) film laminated between two 3 mm thick low-iron float glass panes. The film parameters were chosen in order to simulate the optical properties of a layer functionalized with 300 ppm of Lumogen Red 305 developed by BASF, Ludwigshafen, Germany. The radiative phenomena between surfaces were instead modeled using the "Surface-to-surface Radiation" (RAD) interface, being RAD a physics modeling only surface interactions, the parameters required by COMSOL are the surface emissivity, transmissivity, and reflectivity. However, it is important to underline that the definition of the surface properties depends on different simulation aspects such as the methodology used to model the radiation, the type of surface, and the imposed

boundary conditions. The surfaces inserted in the RAD interface were modeled following the COMSOL application presented in [42]. The LSC optical properties were attributed to the PVB layer by using a boundary material, which was modeled having an emissivity between 0.7 and 0.9 in the range 0–610 nm, and 0.05 for longer wavelengths. These values were used to model the LSC high absorption at shorter wavelengths and its transparency for longer ones. As reported in [43], they were calibrated thanks to a combination of direct measurements and literature values useful for the proper modeling of the panel optical properties. For the cell and the glass emissivity, the values reported by Riverola et al. were used [44], whereas the ambient parameters were measured by an outdoor monitoring station placed in the Ferrara University campus [45], so as to use boundary conditions obtained by on-field measurements (e.g., vertical solar radiation, ambient temperature, convective heat flux). In particular, the simulations were performed by considering a south-facing vertical window, and comparing the configurations displayed in Figure 2. To assess the impact of the PCM on the system, the NOCT of the benchmark configuration having the window frame filled with air was compared to the value obtained for the same configuration in which the air was substituted with a paraffin PCM.

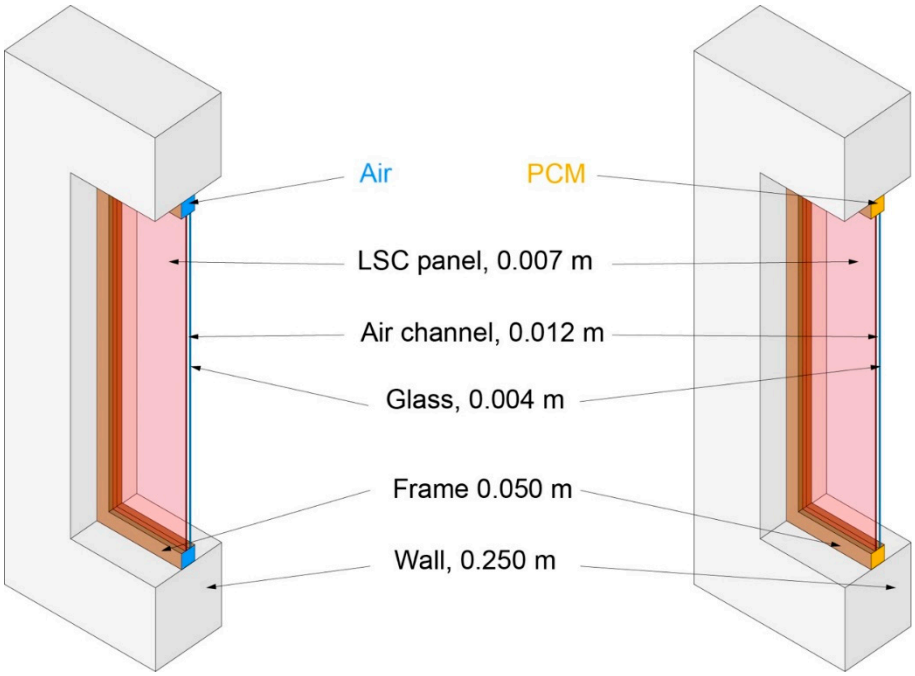

Figure 2. Configurations modeled. Window area 1.4 × 1 m^2.

The optimization of the PCM's thermal properties was primarily focused on its melting temperature, with latent heat serving as a secondary variable to evaluate the impact of different PCM thermal masses on NOCT. Both single-day and multi-day simulations were performed. Single-day simulations helped in narrowing down the range of optimal melting temperatures by considering seasonal variations in NOCT between summer and winter. Multi-day simulations were then used to select melting temperatures that not only reduced NOCT but also ensured its long-term stability. Indeed, during PCM charging hours, the heat produced by the PV module is stored by the PCM while undergoing the phase transition (solid to liquid). However, if this phase change is not fully reversed during the discharging phase—meaning the PCM does not completely solidify overnight—the material's capacity to absorb heat during the following day is progressively diminished. This reduction in thermal mass results in a gradual decrease in PCM cooling effect, leading to a steady increase in NOCT over time, as less heat is absorbed and stored with each day–night cycle.

3. Results and Discussion

The vertical irradiance impinging on the PV window and ambient temperature used as boundary conditions in the simulations are shown in Figure 3. Figure 3 also reports NOCT in absence of PCM, which was used as the main parameters to optimize the PCM properties.

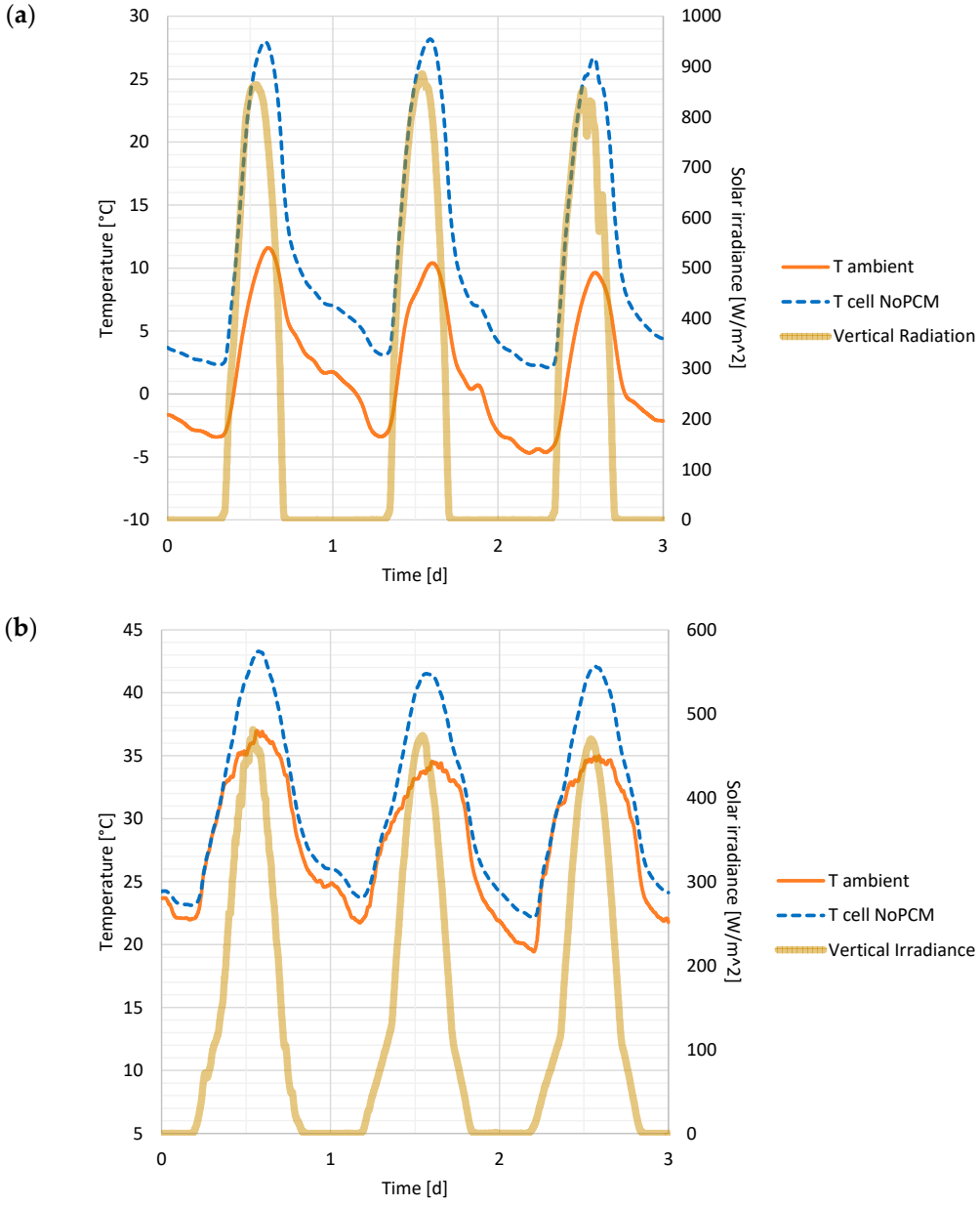

Figure 3. Thermodynamic variables used to optimize PCM properties, including the boundary conditions imposed to the numerical models, ambient temperature and vertical radiation, and NOCT in absence of PCM in summer (**a**), and winter (**b**).

During the preliminary optimization phase, single-day simulations were conducted varying the PCM melting temperature between 20 °C and 42 °C and considering three Δh values. The upper limit of 42 °C was chosen because the maximum temperature reached by the PV arrays without PCM was ~43 °C, making higher melting temperatures ineffective for cooling the solar cells. The lower boundary of 20 °C was selected to ensure that the system could also be optimized for winter conditions. The temperature parametrization was combined with a variation in PCM latent heat. In Figure 4, the results related to simulations conducted during summertime are presented. As expected, the increment of

latent heat increases the system thermal inertia, as materials with higher latent heat absorb or release more energy during phase changes without significant temperature variation. This enhances their ability to contain and delay temperature fluctuations, making them highly effective for stabilizing thermal conditions. Nevertheless, PCMs having a melting temperature below 32 °C have proven to be inadequate for the reduction in NOCT during cooling season. Indeed, the liquid fraction of PCMs simulated with a melting temperature below 32 °C was still above 80% after a whole working day, thus preventing the PCM from the complete discharge during night hours independently on the selected Δh.

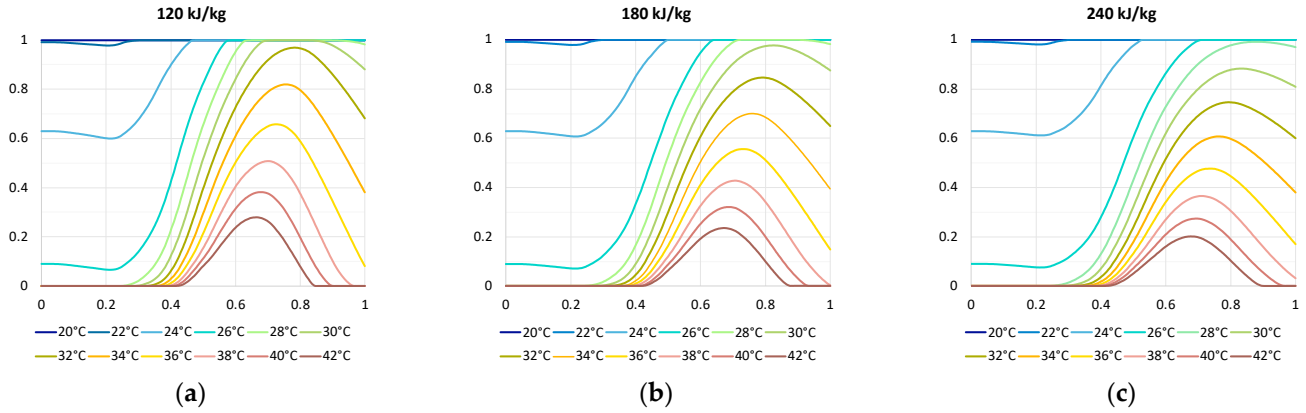

Figure 4. PCM liquid fraction as function of the different melting temperatures, 120 kJ/kg (**a**), 180 kJ/kg (**b**), and 240 kJ/kg (**c**) (summer simulations).

Considering the NOCT values reported in Figure 3a, melting temperatures above 30 °C are hardly compatible with effective exploitation during winter. Analyzing the operating temperatures reached by the cells across seasons, it is evident that reducing temperatures in summer results in a greater performance improvement compared to similar reductions in winter when evaluated against performance under Standard Test Conditions (STC). During winter, the maximum NOCT is approximately 28 °C, whereas in summer, it reaches values above 43 °C. This significant difference provides more opportunity for performance enhancements through temperature control during the summer months; therefore, the PCM properties were specifically optimized to reduce NOCT during the cooling season.

Furthermore, considering the seasonal variations in vertical irradiation, optimizing temperature control for summer conditions ensures greater uniformity in the photovoltaic window's energy production throughout the year. This uniformity is crucial for the effective integration of renewable energy generation into the electricity grid [46].

Based on summer boundary conditions, a secondary optimization step was performed, in which melting temperatures ranging from 32 °C to 42 °C were investigated. This time, multi-day simulations were performed allowing the PCM to extend its discharge cycle until dawn the following day, or even further.

From the results reported in Figure 5, it is evident how PCMs having melting temperatures below 34 °C are inadequate for the application presented in this paper, as the PCM does not completely solidify before the charging cycle of the next day, thus reducing its heat sink properties. Moreover, for latent heat equal to 240 kJ/kg, the minimum melting temperature raises up to 36 °C (see Figure 5c), due to the higher thermal inertia of the material. The melting temperatures from 36 °C to 42 °C were considered optimal for the application presented in this paper, and their impact on the NOCT was evaluated.

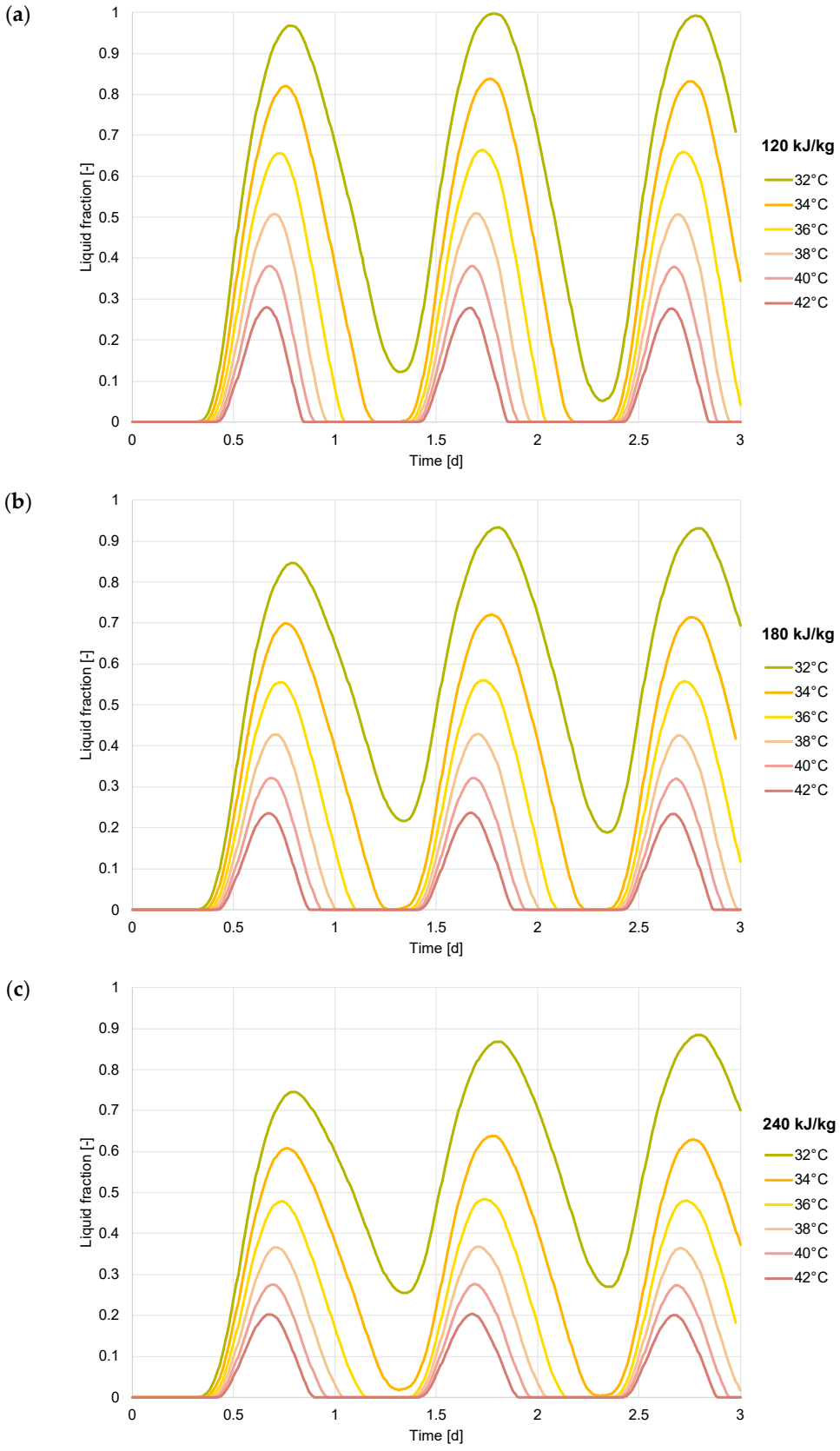

Figure 5. PCM liquid phase as a function of different melting temperatures and latent heat, considering multi-day simulations. 120 kJ/kg (**a**), 180 kJ/kg (**b**), and 240 kJ/kg (**c**).

In Figure 6, a comparison of the various NOCTs as a function of both the PCM melting temperatures and latent heat capacity is presented. As expected, the integration of PCM helps controlling NOCT if compared to the scenario where no PCM is used. Furthermore, materials with higher latent heat capacity provide more effective thermal regulation ensuring lower cell temperatures during the operational phase of the LSC panel. The differences in NOCT values are summarized in Table 2. During nighttime, the PCM releases the heat stored during the day, solidifying and thus leading to higher temperatures in the PV array if compared to the reference case. However, this is not a concern, as the cells are inactive during nighttime and the temperatures observed remain well below the NOCT typically experienced by PV panels in real-world conditions.

The results indicate that PCM effectively reduces the peak temperature and delays the temperature peak. At 120 kJ/kg, the delay is 1 h, 33 min, and this extends to 1 h, 56 min, for a latent heat of 180 kJ/kg. The corresponding temperature reductions are −4.2 °C and −5.3 °C, respectively. This clearly shows that increasing the latent heat of the PCM results in both a longer delay in temperature rise and a greater reduction in temperature compared to the case without PCM. The PCM with higher latent heat absorbs more thermal energy before transitioning phases, resulting in better thermal performance, especially for the 36 °C melting temperature. For PCM with a melting temperature of 38 °C, the trend is similar. The temperature delay at 120 kJ/kg is 1 h, 43 min, which increases to 1 h, 49 min at 240 kJ/kg. The corresponding temperature reductions range from −3.9 °C to −5.1 °C. As with the 36 °C PCM, the increase in latent heat improves the PCM's ability to both delay the temperature rise and reduce the overall temperature. Although the increase in delay is less significant compared to the 36 °C PCM, the general trend of enhanced thermal regulation with higher latent heat is consistent.

For PCM with a melting temperature of 40 °C, the delay is 1 h, 23 min at 120 kJ/kg, increasing only slightly to 1 h, 25 min at 240 kJ/kg. The temperature reductions for the investigated Δh are −3.3 °C, −3.87 °C, and −4.1 °C. While there is a noticeable improvement in cooling performance with increasing latent heat, the temperature delay does not increase as much as for the lower melting temperatures. This suggests that, although the 40 °C PCM can still benefit from higher latent heat, its ability to significantly delay the temperature rise is limited compared to PCMs with lower melting points. The PCM with a melting temperature of 42 °C shows the smallest delay and temperature reduction across the three latent heat capacities. The delay starts at 46 min at 120 kJ/kg, increasing to 1 h, 10 min at 240 kJ/kg. Similarly, the temperature reduction begins at −2.7 °C and increases to −3.37 °C. The comparatively smaller delay and cooling effect indicate that the 42 °C PCM is less effective overall, even when the latent heat is increased. While higher latent heat does improve performance to some extent, PCM's higher melting temperature inherently limits its ability to provide the same level of thermal regulation as the lower melting point materials.

To assess how the NOCT reduction impacts the power output of each photovoltaic branch, an IV curve, a real PV array manufactured for large-area LSC panels, was used as reference. This IV curve was measured under STC, and the characteristic curves corresponding to NOCT in the range 36 °C ÷ 42 °C were simulated by using a two-diode model [47]. The range was chosen according to the results reported in Table 2, which proves that the implementation of PCM may reduce the NOCT from a minimum of ~2 °C to a maximum of ~6 °C. Approximating the maximum temperature reached by the cells in absence of the PMC at ~42 °C, 36 °C corresponds to the lower working temperature that appears possible based on the thermal simulations, whereas 40 °C corresponds to the higher one. Figure 7 presents the electrical performance of the selected PV module having an NOCT in the selected range.

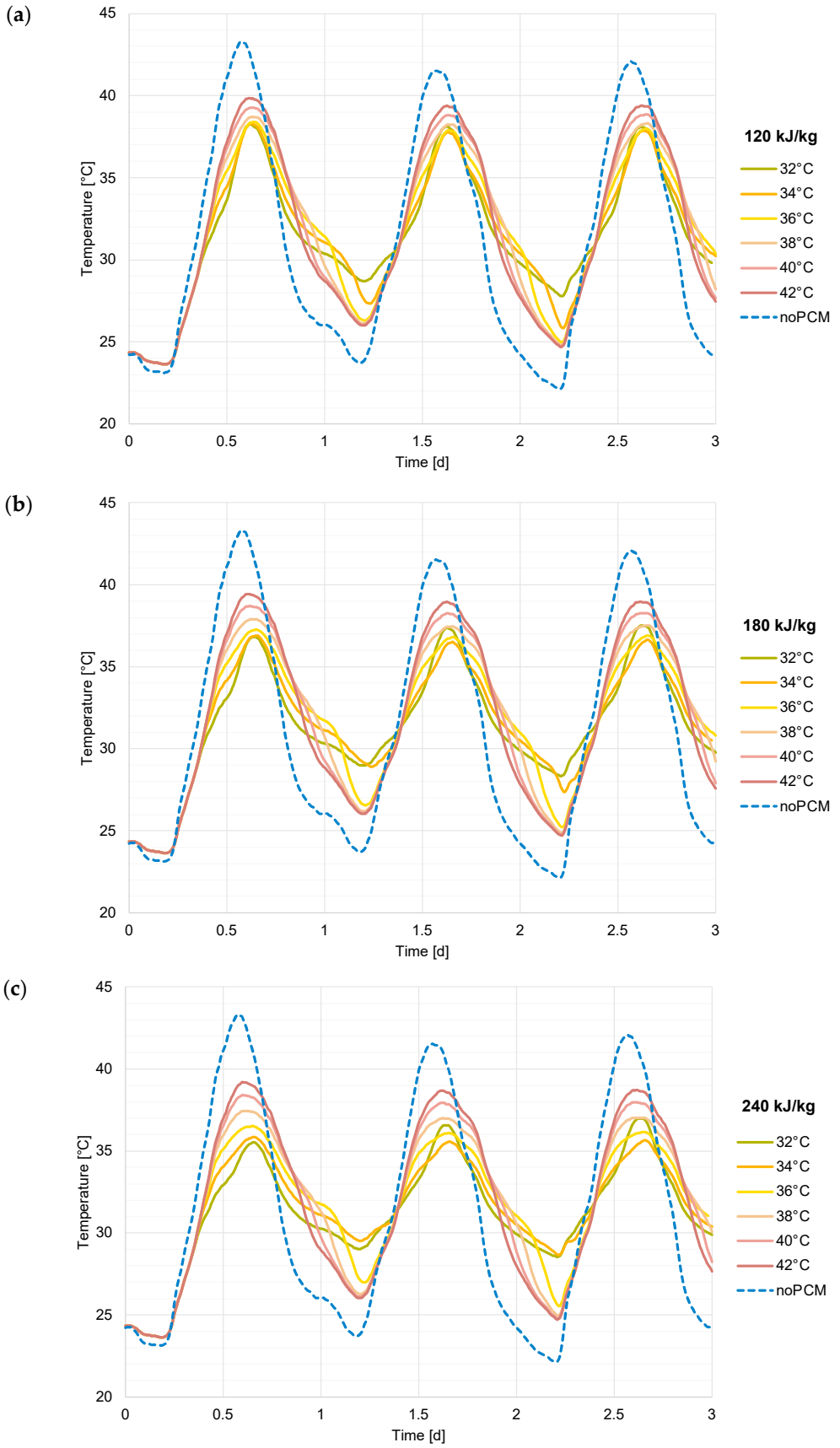

Figure 6. NOCT temperature at different PCM melting temperatures and different latent heat, namely 120 kJ/kg (**a**), 180 kJ/kg (**b**), and 240 kJ/kg (**c**).

Table 2. Impact of PCM introduction on NOCT.

	Temperature Difference			
	PCM Melting 36 [°C]	**PCM Melting 38 [°C]**	**PCM Melting 40 [°C]**	**PCM Melting 42 [°C]**
120 kJ/kg	−4.2	−3.8	−3.2	−2.7
180 kJ/kg	−5.3	−4.6	−3.9	−3.1
240 kJ/kg	−6.0	−5.1	−4.1	−3.3

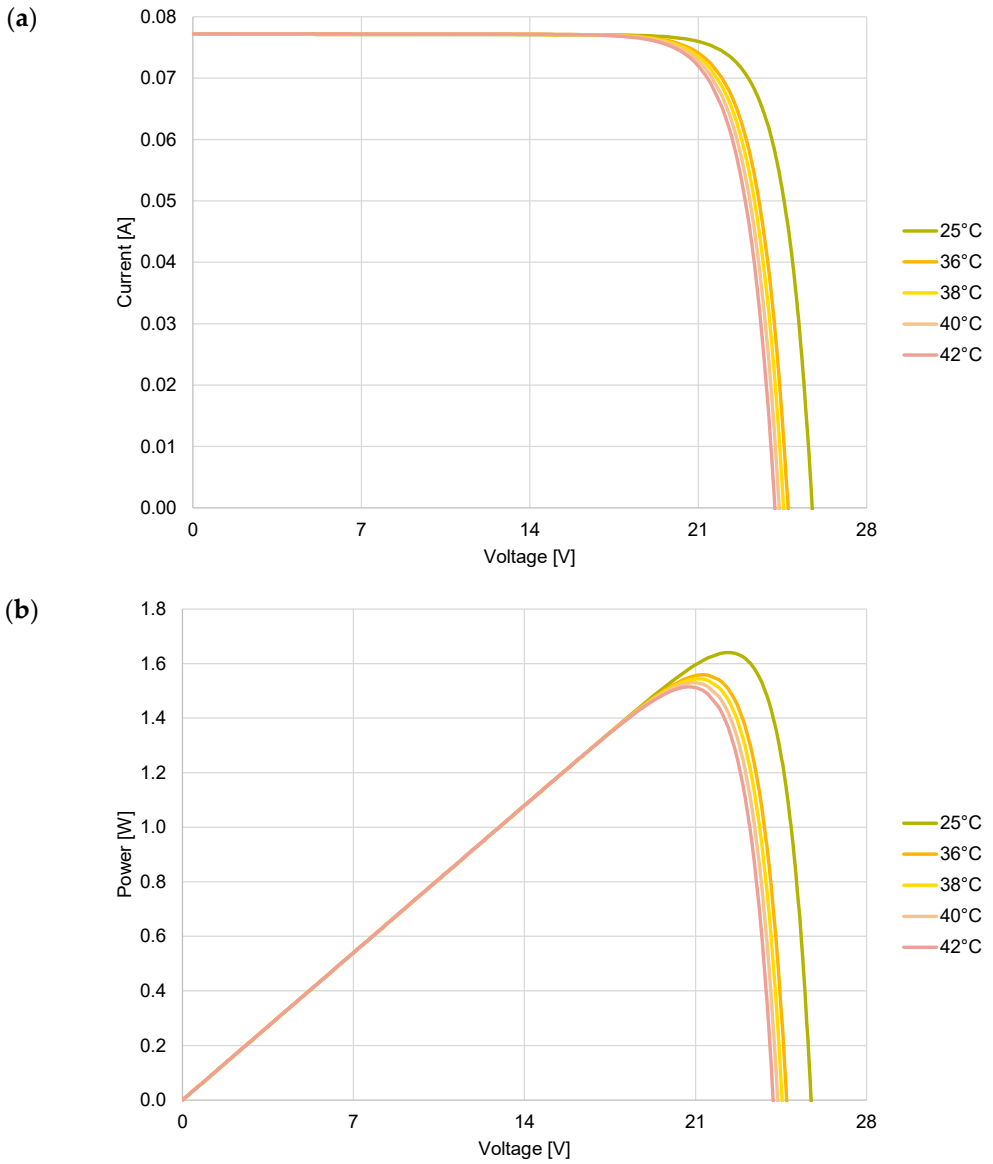

Figure 7. Electrical performance of a PV array depending on the NOCT temperature IV curves (**a**), and PV curves (**b**).

The data presented in Table 3 correspond to the power produced by one of the four PV branches inserted in the PV window, each consisting of 40 monocrystalline silicon PERC cells [48]. Specifically, the last column of Table 3 presents the increase in the power produced by the PV array thanks to the lower NOCT having as a reference NOCT 42 °C. Since the system consists of four identical photovoltaic arrays, the total percentage increase in power across all systems corresponds to 3.94% at 40 °C, 7.88% at 38 °C, and 11.80% at 36 °C. For the NOCT of 25 °C, no power variation has been calculated since the related IV curve was

used to calibrate a simulation based on a two-diode model, allowing for the extraction of the system's physical parameters. This analysis highlights how the reduction in cell temperature leads to a significant increase in power output, with the most pronounced improvement observed at 36 °C.

Table 3. Electrical parameters of a PV array as a function of the NOCT.

NOCT [°C]	V_{oc} [V]	I_{sc} [A]	V_{MPP} [V]	I_{MPP} [A]	P_{MAX} [W]	P_{MAX} [%]
25	25.73	0.077139	22.33	0.073459	1.64	-
36	24.70	0.077187	21.30	0.073203	1.56	2.95
38	24.53	0.077195	21.08	0.073245	1.54	1.97
40	24.35	0.077204	20.87	0.073286	1.53	0.98
42	24.18	0.077212	20.65	0.073327	1.51	0

4. Future Perspective

The work performed by Lizcano et al. [49] highlights how a reduction between 2 °C and 3 °C in the operational temperature of a PV module can extend its lifetime by two years in hot climates and just one year in moderate ones. Therefore, a reduction in the operational temperature of the PV arrays not only increases the electrical performance of a PV module but also has important benefits related to their reliability. This is particularly relevant when considering that the PV arrays of the configuration here presented are encased in window frames, which limits their ability to passively cool through environmental factors such as natural convection and wind. Moreover, due to the heat released by the PCM during its discharge process, the daily thermal gradient experienced by the PV panels is reduced. This decrease in thermal stress caused by day–night cycles further enhances the reliability and longevity of the PV modules [50,51].

In future work, it would be interesting to explore the use of a combination of two PCMs with distinct properties, particularly focusing on materials with a melting temperature tailored for winter months. This approach could enhance the system efficiency during the summer months by providing better thermal regulation and ensuring extended cooling benefits, while offering cooling advantages during winter. This dual-PCM system could lead to year-round thermal management improvements, while enabling more precise regulation of cell temperatures across various seasons, climate zones, and locations.

From an economic perspective, the addition of PCM within the frame does not represent a substantial increase in the overall price of the PV system. Indeed, for the proposed configuration, the mass of PCM needed is equivalent to ~7 kg, and with a price in the range of 2 €/kg to 6 €/kg its addition does not represent a substantial increase in the overall price of the PV window. In any case, the system here presented can be further optimized by using only two photovoltaic receivers; indeed, the results presented by Bernardoni et al. [7] show that this design significantly decreases the cost of the LSC panel, and marginally impacts the PV production.

5. Conclusions

The obtained results testify that the integration of PCMs in PV windows based on LSC technology can effectively increase their power output. A paraffin PCM was integrated in the frame of a south-facing vertical window, and its impact on the working cell temperature was evaluated thanks to finite element simulations. Several melting temperatures and latent heat capacities were investigated, and a clear relationship between the PCM latent heat capacity and its thermal performance has been highlighted. PCMs with higher latent heat can absorb more thermal energy during phase change, leading to longer delays in temperature rise and greater reductions in cell working temperature. The PCM thermal properties were optimized to reduce NOCT in summertime of a temperate subcontinental climate, as considering the environmental and boundary parameters, this approach also ensures two main advantages. Firstly, it offers greater potential for performance improve-

ments with respect to the winter season, due to the higher cell working temperatures. Secondly, it leads to more consistent energy production throughout the year.

The cell temperature reduction ranged from 2.7 °C to 6 °C, with the maximum value corresponding to a melting temperature of 36 °C and a latent heat equal to 240 kJ/kg. The cooling effect of PCM with the same melting temperature but a different latent heat resulted in an NOCT reduction corresponding to 4.2 °C, and 5.3 °C, for values of 120 kJ/kg, and 180 kJ/kg, respectively. Increasing the melting temperature to 38 °C results in a more moderate reduction in cell temperature, which, considering the increasing Δh values, amounts to 3.8 °C, 4.6 °C, and 5.1 °C. When higher melting temperatures are considered (40 °C and 42 °C), the improvement in performance is less evident, and it is limited to the maximum values of 3.3 °C and 4.1 °C when the higher latent heat (240 kJ/kg) is considered. Considering the electrical performance, the 6 °C degree NOCT reduction leads to an increase in power output of 2.95% for each photovoltaic branch, which translates to a total increase of approximately 11.80% across the whole PV window. The simulations having the same latent heat, but a higher melting temperature, 38 °C and 40 °C, led to a total improvement in electricity production that corresponds to 7.88% and 3.94%, respectively. The evidence that even the PCM having a 40 °C melting temperature leads to a contained but not negligible increase in the electricity production of the presented PV window testifies how the coupling between PCMs and semi-transparent PV panels based on LSC technologies may represent a crucial aspect to enhance the overall effectiveness of these systems without impacting on their optical properties.

Author Contributions: Conceptualization, G.M.; methodology, G.M. and E.B.; software, G.M.; validation, G.M. and E.B.; formal analysis, V.D.; investigation, V.D.; data curation, E.B.; writing—original draft preparation, G.M. and E.B.; writing—review and editing, V.D.; visualization, E.B.; supervision, D.V.; project administration, D.V.; funding acquisition, D.V. All authors have read and agreed to the published version of the manuscript.

Funding: This research was funded by the project PNRR ECOSISTER "Ecosystem for Sustainable Transition in Emilia-Romagna", code ECS_00000033, Affiliated Spoke n.2 scientific referent Prof. Donato Vincenzi, FINUE, NextGenEU, M4C2 INV. 1.5.

Institutional Review Board Statement: Not applicable.

Informed Consent Statement: Not applicable.

Data Availability Statement: All relevant data supporting the findings of this study are included within the manuscript, or available from the corresponding author upon reasonable request.

Conflicts of Interest: The authors declare no conflicts of interest.

References

1. Mangherini, G.; Diolaiti, V.; Bernardoni, P.; Andreoli, A.; Vincenzi, D. Review of Façade Photovoltaic Solutions for Less Energy-Hungry Buildings. *Energies* **2023**, *16*, 6901. [CrossRef]
2. Da, Y.; Xuan, Y.; Li, Q. From Light Trapping to Solar Energy Utilization: A Novel Photovoltaic-Thermoelectric Hybrid System to Fully Utilize Solar Spectrum. *Energy* **2016**, *95*, 200–210. [CrossRef]
3. Sadhishkumar, S.; Balusamy, T. Performance Improvement in Solar Water Heating Systems—A Review. *Renew. Sustain. Energy Rev.* **2014**, *37*, 191–198. [CrossRef]
4. Khele, I.; Szabó, M. A Review of the Effect of Semi-Transparent Building-Integrated Photovoltaics on the Visual Comfort Indoors. *Dev. Built Environ.* **2024**, *17*, 100369. [CrossRef]
5. Bernardoni, P.; Mangherini, G.; Andreoli, A.; Diolaiti, V.; Marrazzo, R.; Melchiorre, F.; Zanardi, S.; Vincenzi, D. Design of a Color Neutral Nonpatterned Photovoltaic Window Based on Luminescent Solar Concentrator. *Sol. RRL* **2024**, *8*, 2400195. [CrossRef]
6. De Bruin, T.A.; Van Sark, W.G.J.H.M. Numerical Method for Calculation of Power Conversion Efficiency and Colorimetrics of Rectangular Luminescent Solar Concentrators. *Sol. RRL* **2023**, *7*, 202200787. [CrossRef]
7. Bernardoni, P.; Mangherini, G.; Gjestila, M.; Andreoli, A.; Vincenzi, D. Performance Optimization of Luminescent Solar Concentrators under Several Shading Conditions. *Energies* **2021**, *14*, 816. [CrossRef]
8. Castelletto, S.; Boretti, A. Luminescence Solar Concentrators: A Technology Update. *Nano Energy* **2023**, *109*, 108269. [CrossRef]
9. Sharma, P.; Kolhe, M.; Sharma, A. Economic Performance Assessment of Building Integrated Photovoltaic System with Battery Energy Storage under Grid Constraints. *Renew. Energy* **2020**, *145*, 1901–1909. [CrossRef]

10. Ghosh, A. Fenestration Integrated BIPV (FIPV): A Review. *Sol. Energy* **2022**, *237*, 213–230. [CrossRef]
11. Villa, S.; Out, D.; Guillevin, N.; Hurtado Ellmann, M.; Ribberink, M.; Valckenborg, R. Outdoor Performance Analysis of Semitransparent Photovoltaic Windows with Bifacial Cells and Integrated Blinds. *Sol. RRL* **2024**, *8*, 2400515. [CrossRef]
12. De Bruin, T.A.; Terricabres-Polo, R.; Kaul, A.; Zawacka, N.K.; Prins, P.T.; Gietema, T.F.J.; de Waal, A.C.; de Boer, D.K.G.; Vanmaekelbergh, D.A.M.; Leblans, P.; et al. Analysis of the 1 Year Outdoor Performance of Quantum Dot Luminescent Solar Concentrators. *Sol. RRL* **2023**, *7*, 2201121. [CrossRef]
13. De Bruin, T.A.; Van Sark, W.G.J.H.M. Investigation of Quantum Dot Luminescent Solar Concentrator Single, Double and Triple Structures: A Ray Tracing Simulation Study. *Ceram. Int.* **2023**, *49*, 24454–24468. [CrossRef]
14. Zettl, M.; Mayer, O.; Klampaftis, E.; Richards, B.S. Investigation of Host Polymers for Luminescent Solar Concentrators. *Energy Technol.* **2017**, *5*, 1037–1044. [CrossRef]
15. Rafiee, M.; Chandra, S.; Ahmed, H.; McCormack, S.J. An Overview of Various Configurations of Luminescent Solar Concentrators for Photovoltaic Applications. *Opt. Mater.* **2019**, *91*, 212–227. [CrossRef]
16. Li, S.; Haussener, S. Radiative Transfer in Luminescent Solar Concentrators. *J. Quant. Spectrosc. Radiat. Transf.* **2024**, *319*, 108957. [CrossRef]
17. Liu, H.; He, W.; Liu, X.; Zhu, J.; Yu, H.; Hu, Z. Building Integrated Concentrating Photovoltaic Window Coupling Luminescent Solar Concentrator and Thermotropic Material. *Energy* **2023**, *284*, 129237. [CrossRef]
18. Harahap, R.; Suherman, S. Active Versus Passive Cooling Systems In Increasing Solar Panel Output. In Proceedings of the Environmental Innovations: Advances in Engineering, Technology and Management, EIAETM, Online, 19–23 October 2020; pp. 157–166.
19. Nižetić, S.; Giama, E.; Papadopoulos, A.M. Comprehensive Analysis and General Economic-Environmental Evaluation of Cooling Techniques for Photovoltaic Panels, Part II: Active Cooling Techniques. *Energy Convers. Manag.* **2018**, *155*, 301–323. [CrossRef]
20. Ortiz Lizcano, J.C.; Ziar, H.; de Mooij, C.; Verheijen, M.P.F.; van Nierop Sanchez, C.; Ferlito, D.; Connelli, C.; Canino, A.; Zeman, M.; Isabella, O. Long-Term Experimental Testing of Phase Change Materials as Cooling Devices for Photovoltaic Modules. *Sol. Energy Mater. Sol. Cells* **2024**, *277*, 113133. [CrossRef]
21. Dutil, Y.; Rousse, D.R.; Salah, N.B.; Lassue, S.; Zalewski, L. A Review on Phase-Change Materials: Mathematical Modeling and Simulations. *Renew. Sustain. Energy Rev.* **2011**, *15*, 112–130. [CrossRef]
22. Kant, K.; Shukla, A.; Sharma, A.; Biwole, P.H. Heat Transfer Studies of Photovoltaic Panel Coupled with Phase Change Material. *Sol. Energy* **2016**, *140*, 151–161. [CrossRef]
23. Afaynou, I.; Faraji, H.; Choukairy, K.; Arıcı, M.; Khallaki, K. Heat Transfer Improvement of Phase Change Materials by Metal Foams and Nanoparticles for Efficient Electronic Thermal Management: A Comprehensive Study. *Int. J. Heat Mass Transf.* **2024**, *227*, 125534. [CrossRef]
24. Stropnik, R.; Stritih, U. Increasing the Efficiency of PV Panel with the Use of PCM. *Renew. Energy* **2016**, *97*, 671–679. [CrossRef]
25. Tao, M.; Zhenpeng, L.; Jiaxin, Z. Photovoltaic Panel Integrated with Phase Change Materials (PV-PCM): Technology Overview and Materials Selection. *Renew. Sustain. Energy Rev.* **2019**, *116*, 109406. [CrossRef]
26. Preet, S. A Review on the Outlook of Thermal Management of Photovoltaic Panel Using Phase Change Material. *Energy Clim. Chang.* **2021**, *2*, 100033. [CrossRef]
27. Baccega, E.; Bottarelli, M.; Gallero González, J.F.; Zannoni, G. Improving Energy Efficiency of a Ventilated Tiled Roof by Using Phase Change Materials. *Sustain. Energy Technol.* **2022**, *1*, 338–346.
28. Mellor, A.; Alonso Alvarez, D.; Guarracino, I.; Ramos, A.; Riverola Lacasta, A.; Ferre Llin, L.; Murrell, A.J.; Paul, D.J.; Chemisana, D.; Markides, C.N.; et al. Roadmap for the Next-Generation of Hybrid Photovoltaic-Thermal Solar Energy Collectors. *Sol. Energy* **2018**, *174*, 386–398. [CrossRef]
29. Baccega, E.; Bottarelli, M.; Su, Y. Alternative Experimental Characterization of Phase Change Material Plasterboard Using Two-Step Temperature Ramping Technique. *Energy Build.* **2022**, *267*, 112153. [CrossRef]
30. Maghrabie, H.M.; Mohamed, A.S.A.; Fahmy, A.M.; Abdel Samee, A.A. Performance Enhancement of PV Panels Using Phase Change Material (PCM): An Experimental Implementation. *Case Stud. Therm. Eng.* **2023**, *42*, 102741. [CrossRef]
31. Xu, Z.; Kong, Q.; Qu, H.; Wang, C. Cooling Characteristics of Solar Photovoltaic Panels Based on Phase Change Materials. *Case Stud. Therm. Eng.* **2023**, *41*, 102667. [CrossRef]
32. Mathew, M.P.; Harikrishnan, R.; Thomas, A.S.; Salim, S. Experimental Study of Heat Transfer Characteristics of Phase Change Material-Filled Glazed Windows. *Mater. Today Proc.* **2022**. *In Press, Corrected Proof.* [CrossRef]
33. Jalil, J.M.; Salih, S.M. Experimental and Numerical Investigation of Paraffin Wax as Thermal Insulator in a Double Glazed Window. *J. Energy Storage* **2021**, *35*, 102173. [CrossRef]
34. Che-Pan, M.; Simá, E.; Ávila-Hernández, A.; Uriarte-Flores, J.; Vargas-López, R. Thermal Performance of a Window Shutter with a Phase Change Material as a Passive System for Buildings in Warm and Cold Climates of México. *Energy Build.* **2023**, *281*, 112775. [CrossRef]
35. Zhao, S.; Ming, T.; Wu, Y.; Cai, C.; Yin, K.; Fang, Y.; de Richter, R.; Chen, Y.; Zhou, N. Application Research and Effectiveness Analysis of Phase Change Materials in Building Envelope: A Review. *Energy Build.* **2024**, *324*, 114923. [CrossRef]
36. Karthick, A.; Kalidasa Murugavel, K.; Ghosh, A.; Sudhakar, K.; Ramanan, P. Investigation of a Binary Eutectic Mixture of Phase Change Material for Building Integrated Photovoltaic (BIPV) System. *Sol. Energy Mater. Sol. Cells* **2020**, *207*, 110360. [CrossRef]

37. Karthick, A.; Murugavel, K.K.; Ramanan, P. Performance Enhancement of a Building-Integrated Photovoltaic Module Using Phase Change Material. *Energy* **2018**, *142*, 803–812. [CrossRef]
38. Park, K.E.; Kang, G.H.; Kim, H.I.; Yu, G.J.; Kim, J.T. Analysis of Thermal and Electrical Performance of Semi-Transparent Photovoltaic (PV) Module. *Energy* **2010**, *35*, 2681–2687. [CrossRef]
39. Peng, J.; Curcija, D.C.; Thanachareonkit, A.; Lee, E.S.; Goudey, H.; Selkowitz, S.E. Study on the Overall Energy Performance of a Novel C-Si Based Semitransparent Solar Photovoltaic Window. *Appl. Energy* **2019**, *242*, 854–872. [CrossRef]
40. Ghamari, M.; Sundaram, S. Solar Window Innovations: Enhancing Building Performance through Advanced Technologies. *Energies* **2024**, *17*, 3369. [CrossRef]
41. Mittal, U.; Hattar, M.; Dube, A. A Simulation on Incorporation of PCM in TLSC for Optimum Efficiency of the System. In Proceedings of the 12th IEEE International Conference Electronics, Energy, Environment, Communication, Computer, Control (E^3-C^3), New Delhi, India, 17–20 December 2015; INDICON 2015. pp. 1–5. [CrossRef]
42. COMSOL Greenhouse Effect. Available online: https://www.comsol.it/model/greenhouse-effect-98061 (accessed on 7 December 2024).
43. Mangherini, G.; Bernardoni, P.; Baccega, E.; Andreoli, A.; Diolaiti, V.; Vincenzi, D. Design of a Ventilated Façade Integrating a Luminescent Solar Concentrator Photovoltaic Panel. *Sustainability* **2023**, *15*, 9146. [CrossRef]
44. Riverola, A.; Mellor, A.; Alonso Alvarez, D.; Ferre Llin, L.; Guarracino, I.; Markides, C.N.; Paul, D.J.; Chemisana, D.; Ekins-Daukes, N. Mid-Infrared Emissivity of Crystalline Silicon Solar Cells. *Sol. Energy Mater. Sol. Cells* **2018**, *174*, 607–615. [CrossRef]
45. Bottarelli, M.; Baccega, E.; Cesari, S.; Emmi, G. Role of Phase Change Materials in Backfilling of Flat-Panels Ground Heat Exchanger. *Renew. Energy* **2022**, *189*, 1324–1336. [CrossRef]
46. Tejero-Gómez, J.A.; Bayod-Rújula, Á.A. Analysis of Photovoltaic Plants with Battery Energy Storage Systems (PV-BESS) for Monthly Constant Power Operation. *Energies* **2023**, *16*, 4909. [CrossRef]
47. Tifidat, K.; Maouhoub, N.; Benahmida, A.; Ezzahra Ait Salah, F. An Accurate Approach for Modeling I-V Characteristics of Photovoltaic Generators Based on the Two-Diode Model. *Energy Convers. Manag. X* **2022**, *14*, 100205. [CrossRef]
48. SunPower Technical Data Sheet: C50 Solar Cell Mono Crystalline Silicon 2010. Available online: https://cdn.enfsolar.com/Product/pdf/Cell/5b91fcf3916df.pdf?_ga=2.129740875.699501378.1555670092-1288217596.1555670091 (accessed on 24 October 2024).
49. Lizcano, J.C.O.; Kaaya, I.; Ziar, H.; da Silva, P.S.; Zhou, Y.; Zeman, M.; Isabella, O. Practical Design of an Optical Filter for Thermal Management of Photovoltaic Modules. *Prog. Photovolt. Res. Appl.* **2024**, *32*, 753–773. [CrossRef]
50. Kaaya, I.; Lindig, S.; Weiss, K.A.; Virtuani, A.; Sidrach de Cardona Ortin, M.; Moser, D. Photovoltaic Lifetime Forecast Model Based on Degradation Patterns. *Prog. Photovolt. Res. Appl.* **2020**, *28*, 979–992. [CrossRef]
51. Kaaya, I.; Koehl, M.; Mehilli, A.P.; De Cardona Mariano, S.; Weiss, K.A. Modeling Outdoor Service Lifetime Prediction of PV Modules: Effects of Combined Climatic Stressors on PV Module Power Degradation. *IEEE J. Photovolt.* **2019**, *9*, 1105–1112. [CrossRef]